CrystEngComm

Accepted Manuscript

This article can be cited before page numbers have been issued, to do this please use: S. Yang, S. Wang, H. Xu, D. Zhao, P. Ou and B. Cao, *CrystEngComm*, 2025, DOI: 10.1039/D5CE00591D.

ROYAL SOCIETY OF CHEMISTRY

rsc.li/crystengcomm

View Article Online
DOI: 10.1039/D5CE00591D

Quantum-Dot ZnO-$CsPbBr_3$ Interlayer Induced High-Performance ZnO Nanoarrays/$CsPbBr_3$ Photodetector

Shuhua Yang[a,*], Song Wang [a], Huiyan Xu[b], Degang Zhao[a], Ping Ou [c,*], Bingqiang Cao[a,*]

[a] Materials Center for Energy and Photoelectrochemical Conversion, School of Material Science and Engineering, University of Jinan, Jinan 250022, China

[b] Institute for Smart Materials & Engineering, University of Jinan, Jinan 250022, China.

[c] Guangxi Key Laboratory of Advanced Structural Materials and Carbon Neutralization, Guangxi Colleges and Universities Key Laboratory of Environmental-friendly Materials and Ecological Restoration, School of Materials and Environment, Guangxi Minzu University, Nanning 530105, China

*Corresponding author:

E-mail: yangshuhua78@163.com (Shuhua Yang)

opyp@163.com (Ping Ou)

mse_caobq@ujn.edu.cn (Bingqiang Cao)

View Article Online
DOI: 10.1039/D5CE00591D

Abstract: Recent advances in halide perovskite quantum dot (QD) photodetectors based ZnO nanoarrays (ZnO NRs) have been constrained by significant non-radiative recombination losses at quantum dot interfaces. To address this challenge, an innovative device architecture combining with a tailored quantum-dot (Q-D) $CsPbBr_3$-ZnO composite (P-ZnO) interlayer was designed. The vertically oriented ZnO nanoarrays function as high-mobility electron highways, while the optimized P-ZnO interlayer simultaneously enhances photon harvesting and minimizes interfacial recombination losses. The photodetector incorporating the optimized P-ZnO interlayer demonstrates exceptional performance characteristics, achieving a current modulation ratio exceeding 10^3, a photoresponsivity of 99.73 mA/W, and a specific detectivity reaches to 6.08×10^{11} Jones under 450 nm illumination. Also, the P-ZnO nanocomposite layer enables a remarkable suppression of dark current to 0.423 nA while simultaneously boosting photocurrent generation to 1.166 μA. This work establish a facile and scalable fabrication approach for engineering high-efficiency perovskite quantum dot photodetectors.

Keywords: ZnO nanoarrays; $CsPbBr_3$ quantum dots; composite interlayer; photodetector; charge transport.

View Article Online
DOI: 10.1039/D5CE00591D

1. Introduction

Photodetectors have become indispensable components across diverse technological domains, ranging from advanced defense systems to commercial optoelectronic applications, owing to their exceptional light-to-signal conversion capabilities[1-8]. $CsPbBr_3$ quantum dots (QDs) have distinguished themselves among photoactive nanomaterials for optoelectronic device engineering [9-10], owing to their exceptional combination of quantum-size-effect-tunable optical properties, excellent solution processability for scalable fabrication, and competitive cost-effectiveness compared to conventional semiconductors. These remarkable properties have catalyzed substantial scientific investigation into both the preparation methodologies and practical implementations of $CsPbBr_3$ quantum dots. The most prevalent synthetic routes currently employed are hydrothermal techniques and single-pot colloidal approaches [11-13]. Additionally, strategic manipulation of surface ligands via exchange reactions and chemical modifications has proven effective for constructing optimized quantum dot-based hybrid nanoarchitectures with enhanced performance characteristics[14-16].

From a charge transport perspective, $CsPbBr_3$ quantum dots suffer from inherent limitations[17-19], with experimental Hall effect measurements revealing hole mobilities of 0.1-5 $cm^2\ V^{-1}\ s^{-1}$ and electron mobilities of 2-10 $cm^2\ V^{-1}\ s^{-1}$ - values that are orders of magnitude lower than those required for high-speed optoelectronic applications, ultimately governing the performance ceiling of QD-based devices. To overcome this charge transport constraint, researchers have developed hybrid architectures that

View Article Online
DOI: 10.1039/D5CE00591D

combine $CsPbBr_3$ with high-mobility semiconductors[20-21]. Zinc oxide (ZnO) has emerged as a particularly attractive candidate, possessing both a wide direct bandgap (3.37 eV) and strong excitonic effects (binding energy ~60 meV) at room temperature [22-23]. However, conventional ZnO thin-film configurations present inherent challenges. Their polycrystalline nature introduces numerous interfacial trap states that act as recombination centers, significantly compromising the performance of ZnO-based heterojunction devices. This has led to growing interest in employing ZnO nanoarrays (NRs) for performance enhancement. The one-dimensional nanostructure offers rapid electron transport through direct conduction pathways that minimizes carrier recombination, and substantially improved photoelectric conversion efficiency. Moreover, the combination of high surface area and excellent charge transfer characteristics makes ZnO NRs particularly suitable for constructing high-performance photodetectors. The anisotropic morphology of NRs facilitates efficient carrier collection while maintaining good optical transparency, representing an ideal platform for hybrid photodetector architectures. Although the charge separation efficiency was enhanced greatly by ZnO NRs, the improved performance is still limited.

In this work, a novel ZnO nanoarrays/$CsPbBr_3$ photodetector integrated with a quantum-dot (Q-D) $CsPbBr_3$-ZnO composite (P-ZnO) interlayer (ITO/ZnO NRs/P-ZnO /P/Ag) was developed. In this configuration, the vertically aligned ZnO nanoarrays function as a high-mobility electron transport layer (ETL), while the $CsPbBr_3$ QDs serve as an efficient photon-harvesting medium. The engineered P-ZnO interlayer plays dual critical roles: (1) it creates a three-dimensional interconnected network that

View Article Online
DOI: 10.1039/D5CE00591D

dramatically increases the heterojunction interface area between the ZnO ETL and $CsPbBr_3$ absorption layer, thereby enhancing photon capture probability; and (2) it serves as both a surface passivation layer that suppresses non-radiative recombination in the QD film and an auxiliary charge transport pathway that facilitates efficient electron-hole separation. This synergistic combination of optimized light absorption, enhanced charge separation, and minimized recombination losses results in significantly improved photoelectric conversion efficiency compared to conventional architectures.

2. Experimental

2.1. Preparation of ZnO nanoarrays

The ZnO nanoarrays (NRs) were synthesized through a sequential process beginning with FTO substrate preparation, where 1.5×1.5 cm^2 pieces were ultrasonically cleaned in glass detergent, deionized water, acetone, and ethanol (15 min each), dried under N_2, and UV-ozone treated for 30 min to enhance surface activity. A ZnO seed layer was then deposited by spin-coating (2000 rpm, 30 s) a precursor solution containing zinc acetate dihydrate (2 g), ethanolamine (0.4 mL), and 2-methoxyethanol (40 mL), followed by annealing at 380°C for 1 h. For hydrothermal growth, the seeded substrates were immersed in an aqueous solution of zinc nitrate hexahydrate (20 mM) and hexamethylenetetramine (20 mM) at 95°C for 90 min in a Teflon-lined autoclave. The resulting ZnO NRs were rinsed with deionized water, dried at 60°C for 24 h. The $CsPbBr_3$ QDs (Figure S1,2) and ZnO QDs were prepared according to the method we reported previously (Material synthesis in Supplementary

View Article Online
DOI: 10.1039/D5CE00591D

Information)[24].

2.2. Fabrication of device (ITO/ZnO NRs/P-ZnO/P/Ag)

The photodetectors (ITO/ZnO NRs/P-ZnO/P/Ag) were fabricated through a sequential solution-processing approach (Figure 1): First, 100 μL of P-ZnO composite solution was spin-coated onto ZnO NRs, allowed to wet for 30 s, then spin-coated (2000 rpm, 30 s) and annealed (100°C, 30 min), obtaining P-ZnO interlayer. Subsequently, $CsPbBr_3$ QDs were similarly spin-coated and annealed to form the photoactive layer. Finally, we completed the structure by thermal evaporation of Ag electrodes (100 nm thickness) under high vacuum conditions (<10^{-6} Torr). Control devices (ZnO NRs/P) were prepared identically but without the P-ZnO interlayer.

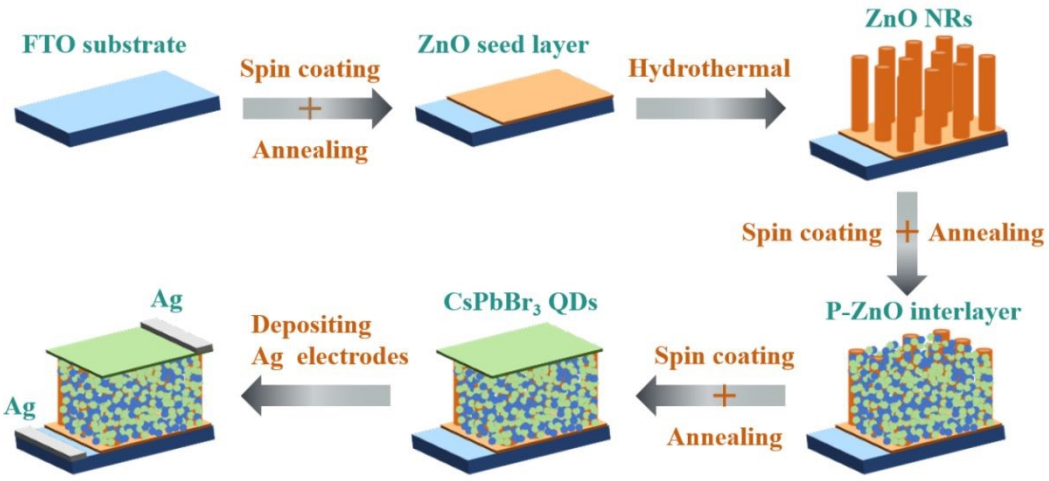

Figure 1. Schematic diagram of the preparation for ITO/ZnO NRs/P-ZnO/P/Ag photodetector.

3. Results and Discussion

The XRD analysis of the synthesized ZnO nanorods reveals well-defined diffraction features characteristic of wurtzite ZnO (PDF#36-1451) (black profile in Figure 2a), with a particularly strong (002) reflection at 34.4°. This pronounced crystallographic orientation indicates the preferential vertical alignment of the nanorods

View Article Online
DOI: 10.1039/D5CE00591D

relative to the substrate surface. Such oriented growth creates an advantageous electron transport scaffold, where the enlarged specific surface area of the nanorod array (compared to conventional ZnO films) significantly enhances the separation efficiency of photogenerated charge carriers. The anisotropic nature of this architecture provides direct conduction pathways while simultaneously increasing the interfacial area available for charge extraction processes. Detailed examination of the ZnO NRs shows well-defined, vertically aligned nanorods with hexagonal wurtzite crystal structure and uniform diameter distribution centered at 50 ± 5 nm (Figure 2b). The high aspect ratio and regular arrangement of these nanostructures create an ideal scaffold for subsequent QD deposition. Notably, the $CsPbBr_3$ QDs form a conformal coating on the ZnO NRs (Figure 2a,c), with complete surface coverage and intimate contact between the two materials. This architecture significantly increases the effective interfacial area compared to planar configurations. The incorporation of the P-ZnO interlayer significantly improves the interfacial integration, as evidenced by the notably denser and more uniform surface coverage shown in Figure 2d. Comparative structural analysis reveals significant enhancement in crystalline quality through the P-ZnO interlayer incorporation (Figure 2a and Figure S2,3), indicating the well compatibility between the $CsPbBr_3$ QDs and ZnO QDs. This engineered interlayer creates an intricate three-dimensional conductive network that bridges the ZnO electron transport layer and $CsPbBr_3$ absorption layer, resulting in a remarkable expansion of the effective heterojunction interface area. The nanostructured architecture enhances light-matter interaction through multiple mechanisms: improved light trapping within the textured

View Article Online
DOI: 10.1039/D5CE00591D

morphology, increased probability of photon absorption at the enlarged interfaces, and optimized charge carrier pathways that minimize recombination losses[24]. This interfacial engineering approach leads to superior optoelectronic performance by simultaneously addressing both optical absorption and electrical transport requirements in the photodetector device.

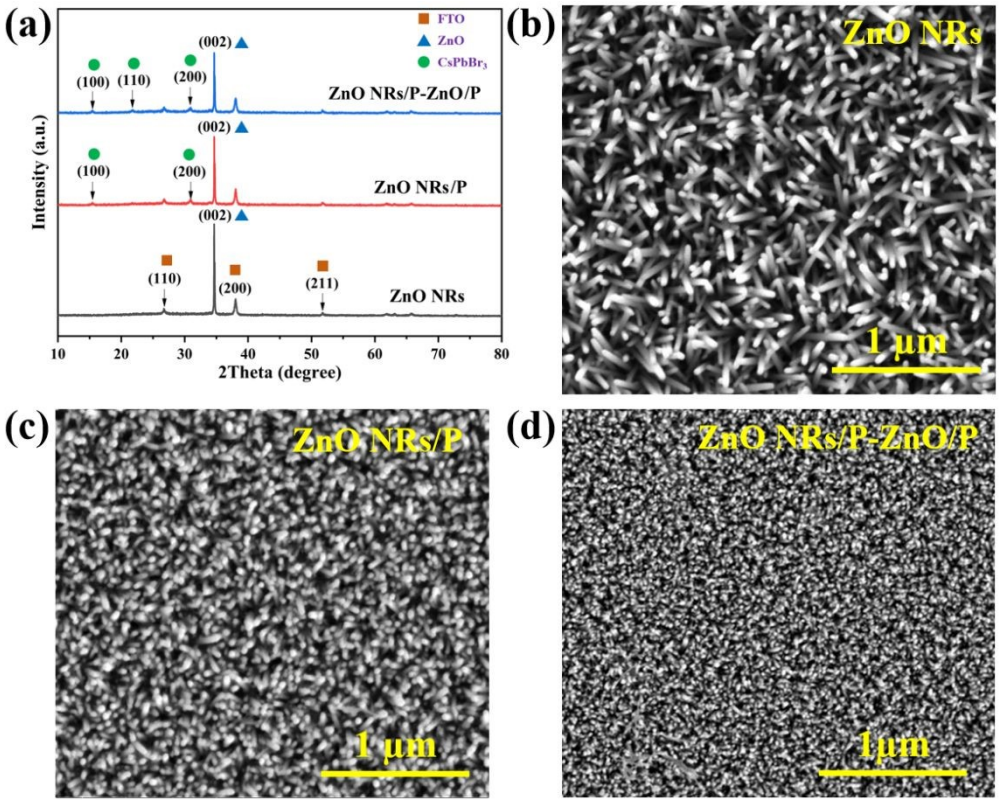

Figure 2. (a) XRD patterns of ZnO NRs, ZnO NRs/P, and ZnO NRs/P-ZnO/P; SEM images of (b) ZnO NRs, (c) ZnO NRs/P, and (d) ZnO NRs/P-ZnO/P.

Figure 3a presents the absorption spectrum and bandgap estimation of ZnO NRs, showing a sharp absorption edge near 384 nm (bandgap ≈ 3.28 eV), in agreement with previous studies[25]. Meanwhile, Figure 3b confirms the high optical transparency of ZnO NRs thin films across the visible spectrum (360–780 nm), reaching 87.5% transmittance at 384 nm. Figure 3c compares the absorption spectra of three $CsPbBr_3$-

View Article Online
DOI: 10.1039/D5CE00591D

based thin films. Pure $CsPbBr_3$ QDs exhibit a pronounced absorbance edge at 512 nm. The ZnO NRs/P composite film demonstrates a slight absorption boost due to quantum size effects, confirming that $CsPbBr_3$ QDs retain their absorption features even within the ZnO framework. Notably, the ZnO NRs/P-ZnO/P spectral profiles demonstrate that integrating a P-ZnO interlayer between the ZnO NRs ETL and $CsPbBr_3$ QD photoactive layer amplifies the absorption intensity at 512 nm. This enhancement promotes electron extraction and accelerates carrier transport, boosting the photodetector's photoelectric conversion efficiency. Figure 3d compares the PL spectra of $CsPbBr_3$-based films under 408 nm excitation. The peaks of ZnO NRs/P and ZnO NRs/P-ZnO/P composites shift slightly to the left, in good agreement with the absorption spectra (Figure 3c). The pure QD film shows the strongest emission, but PL intensity drops sharply when both ZnO NRs ETL and P-ZnO interlayer is introduced. The $CsPbBr_3$ QDs' FWHM (20 nm) matches literature values[26]. The reduced PL peaks in ZnO NRs/P and ZnO NRs/P-ZnO/P composites imply fewer radiative losses and more efficient electron extraction. This results validate the crucial role of both ZnO NRs and P-ZnO interlayer in enhancing the carrier mobility and device efficiency.

View Article Online
DOI: 10.1039/D5CE00591D

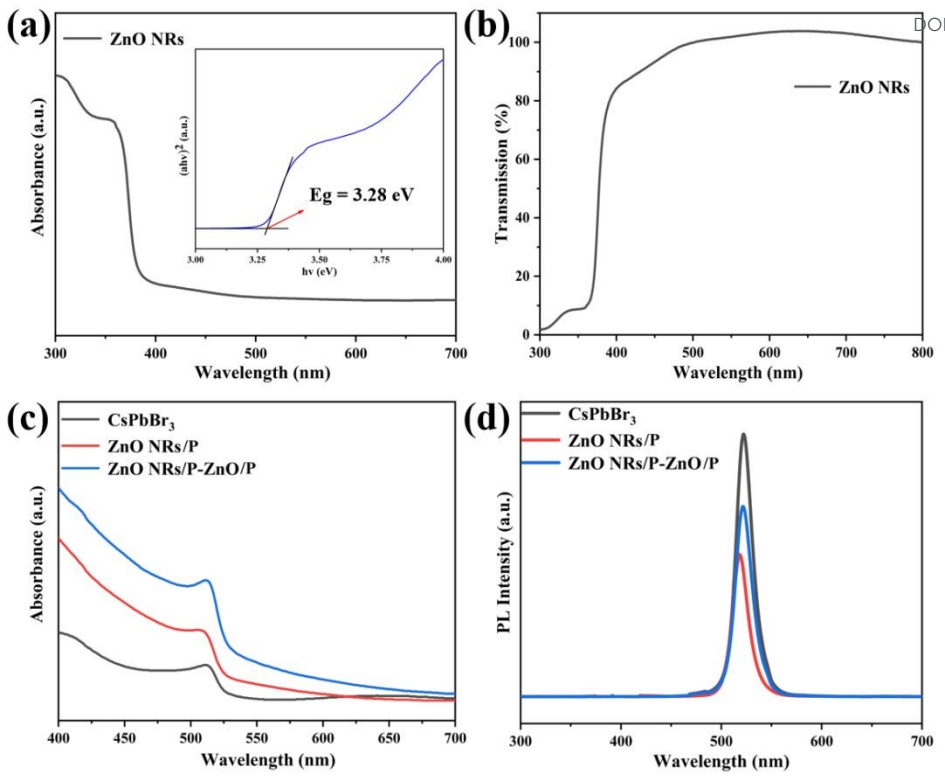

Figure 3. (a) Absorption spectra and (b) transmission spectra of ZnO NRs; (c) Absorption spectra and (d) PL spectra of $CsPbBr_3$, ZnO NRs/P, ZnO NRs/P-ZnO/P thin films.

Two distinct configurations of perovskite QD photodetectors were fabricated for comparative analysis. The first design incorporated a P-ZnO interlayer (referred to as ZnO NRs/P-ZnO/P device), while the second configuration omitted this interlayer (designated as ZnO NRs/P device). Both devices were characterized by measuring their photoresponse properties under 450 nm illumination at ambient temperature. As illustrated in Figure 4a, the ZnO NRs/P-ZnO/P photodetector demonstrated a significantly lower dark current (0.423 nA) compared to the ZnO NRs/P device (1.222 nA). This suppression of dark current in the P-ZnO-modified device can be attributed to the enhanced built-in electric field induced by the P-ZnO interlayer, which effectively impedes spontaneous charge carrier migration under non-illuminated conditions. As demonstrated in Figure 4b, the ZnO NRs/P-ZnO/P photodetector

View Article Online
DOI: 10.1039/D5CE00591D

achieved a markedly higher photocurrent (1.0078 μA), whereas its ZnO NRs/P counterpart displayed comparatively inferior performance. This enhancement is attributed to the P-ZnO interlayer's dual functionality: suppressing nonradiative recombination while simultaneously optimizing interfacial interactions. Specifically, the improved contact interfaces between $CsPbBr_3$ QDs and ZnO QDs, as well as between the P-ZnO interlayer and ZnO NRs, promote enhanced photon absorption, facilitate efficient charge carrier transport, and boost electron-hole pair extraction efficiency, collectively contributing to the superior photoresponse. Figure 4c systematically investigates the current-voltage characteristics of the ZnO NRs/P-ZnO/P photodetector under varying illumination intensities. A monotonic enhancement in photocurrent is observed as the incident light intensity escalates from dark conditions (0 mW cm^{-2}) to 21.56 mW cm^{-2}, consistent with light-driven excitation of additional electron-hole pairs. Complementary temporal response analysis (Figure 4d) reveals superior optoelectronic performance in the P-ZnO-modified device compared to the ZnO NRs/P control. This pronounced improvement in photoresponsivity underscores the critical role of the P-ZnO interlayer in enhancing interfacial charge dynamics through optimized carrier transport pathways and efficient electron-hole separation. The dynamic photoresponse performance of the ZnO NRs/P-ZnO/P device was rigorously evaluated through dual parametric modulation studies (Figures 4e-f). Intensity-dependent measurements (4.5–21.56 mW/cm^2) revealed exceptional cyclic stability with rapid rise/fall kinetics (Figure 4e), while bias-variable tests (Figure 4f) demonstrated voltage-immune switching fidelity, preserving sub-second response

View Article Online
DOI: 10.1039/D5CE00591D

times across multiple operating voltages. Such bias-resilient behavior highlights the interlayer-engineered interface's capacity to decouple charge extraction efficiency from external field perturbations, a critical advancement for practical photodetector applications.

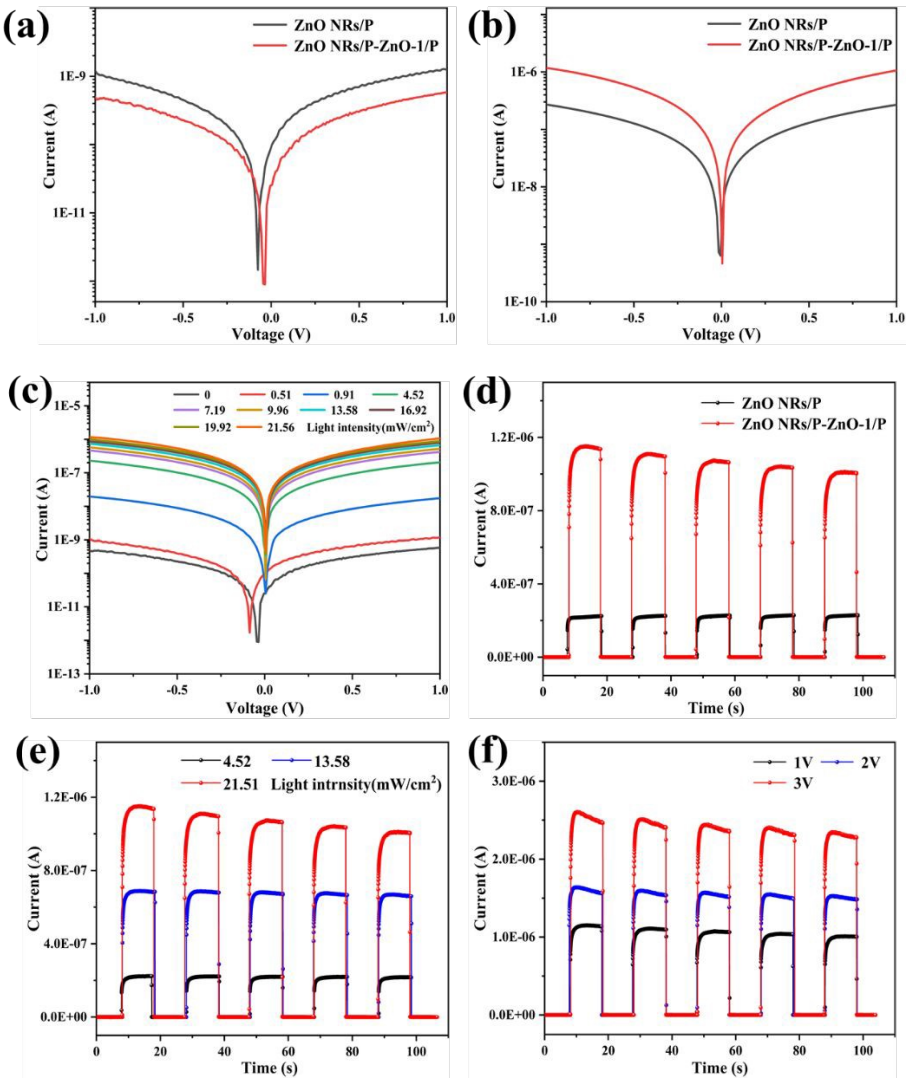

Figure 4. Interlayer-modulated optoelectronic performance: (a,b) Dark/photocurrent and (d) I–T curves contrast between engineered (ZnO NRs/P-ZnO/P) and control (ZnO/P) devices, (c) I-V curves under variable illumination (0-21.56 mW/cm^2), (e,f) Dual-parameter response dynamics: intensity-linear switching (4.5-21.56 mW/cm^2) and bias-stable kinetics (0.5-2.0 V).

To comprehensively evaluate the photoresponse performance of the ZnO NRs/P-

View Article Online
DOI: 10.1039/D5CE00591D

ZnO/P quantum dot photodetector, four critical performance metrics were calculated: the on/off ratio, external quantum efficiency (EQE), responsivity (R), and specific detectivity (D*) (Calculations in Supplementary Information). Figure 5a quantifies the illumination-dependent on/off ratio of the photodetector under 450 nm illumination at the light intensities of 0.51, 0.91, 4.52, 7.19, 9.96, 13.58, 16.92, 19.92, and 21.56 mW/cm^2. The observed linear correlation between on/off ratio and incident photon flux across this range ($R^2 > 0.99$) confirms precise light detection capability, achieving a peak switching ratio of ~10^3 at maximum illumination. Complementarily, Figure 5b reveals an inverse relationship between EQE and light intensity, with the EQE peaking at 27.54% under low-intensity operation. This efficiency reduction at higher irradiance levels suggests intensified carrier recombination dynamics under strong photon flux. Figure 5c demonstrates the light-intensity-dependent current responsivity (R) of the photodetector, peaking at 99.73 mA/W under weak illumination (0.51 mW/cm^2). This value progressively stabilizes to 18.01 mA/W at higher intensities (≥4.5 mW/cm^2), indicative of photogenerated carrier saturation effects. Concurrently, Figure 5d reveals an inverse proportionality between D* and incident power density, with the maximum D* reaching 6.08×10^{11} Jones under low-light conditions. Such performance metrics not only validate the device's dual-mode operational capability (high-sensitivity/low-light vs. high-stability/bright-light modes) but also position it competitively against state-of-the-art quantum dot photodetectors reported in recent literature[14, 27-31].

View Article Online
DOI: 10.1039/D5CE00591D

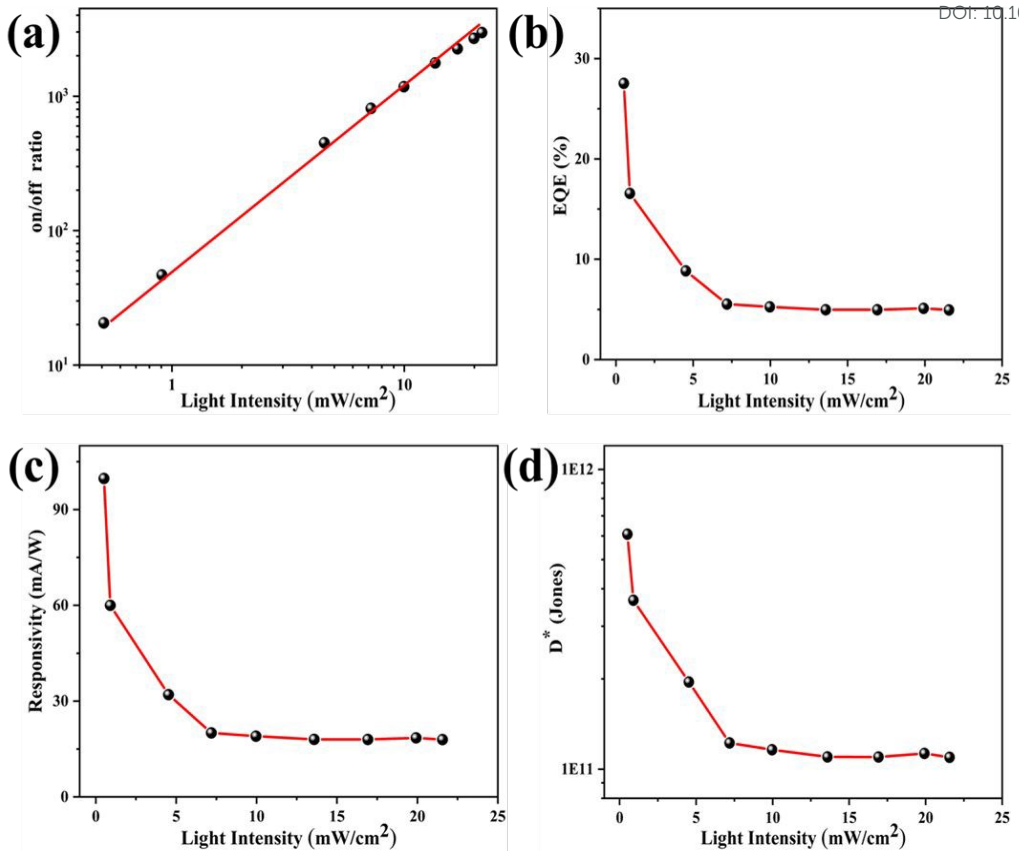

Figure 5. Illumination-intensity-dependent optoelectronic characteristics of the ZnO NRs/P-ZnO/P photodetector at 1 V bias. (a) on/off ratio, (b) EQE, (c) R, (d) D*.

4. Conclusions

In summary, this work demonstrates a significant advancement in perovskite QD photodetectors through quantum-dot-level interfacial engineering of a ZnO/$CsPbBr_3$ hybrid architecture. By integrating vertically aligned ZnO nanoarrays as high-mobility electron highways with a multifunctional P-ZnO composite interlayer, we simultaneously address interfacial recombination losses and charge transport limitations. The optimized device achieves exceptional performance metrics, including a record-low dark current (0.423 nA), high photocurrent (1.166 μA), superior responsivity (99.73 mA/W), and outstanding detectivity (6.08×10^{11} Jones) under 450 nm illumination, while demonstrating robust operational stability across broad light

View Article Online
DOI: 10.1039/D5CE00591D

intensity (4.5–21.56 mW/cm^2) and bias voltage (0.5–2.0 V) ranges. The P-ZnO interlayer's dual functionality—enhancing photon harvesting via 3D interfacial networks and suppressing non-radiative recombination through surface passivation—enables a current modulation ratio exceeding 10^3 and intensity-linear response (R^2 > 0.99). This fully solution-processed architecture not only provides a scalable fabrication strategy but also establishes a universal design paradigm for next-generation optoelectronic devices, with potential extensions to broadband detection and flexible electronics through further compositional and structural engineering.

Conflicts of interest

There are no conflicts to declare.

Acknowledgements

This work is supported by Shandong Provincial Natural Science Foundation (No. ZR2022ME181), National Natural Science Foundation of China (No. 51702123). Shuhua Yang thanks the start-up research funding from University of Jinan.

Reference:

1. Wang, F.; Zhang, T.; Xie, R.; Liu, A.; Dai, F.; Chen, Y.; Xu, T.; Wang, H.; Wang, Z.; Liao, L.; Wang, J.; Zhou, P.; Hu, W., Next-Generation Photodetectors beyond Van Der Waals Junctions. *Adv. Mater.* **2024,** *36* (3), 2301197.

2. Sharma, R.; Henderson, L. N.; Sankar, P.; Tresa, M. M.; Oyeku, O. P.; Perez, E.; Thomas, J., Recent Advancements in Nanomaterials for Near-Infrared to Long-Wave Infrared Photodetectors. *Advanced Optical Materials* **2024,** *12* (35), 2401821.

3. Miao, J.; Zhang, F., Recent progress on highly sensitive perovskite photodetectors. *J. Mater. Chem. C* **2019,** *7* (7), 1741-1791.

4. Sulaman, M.; Song, Y.; Yang, S.; Saleem, M. I.; Li, M.; Perumal Veeramalai, C.; Zhi, R.; Jiang, Y.; Cui, Y.; Hao, Q., Interlayer of PMMA doped with Au nanoparticles for high-performance tandem photodetectors: A solution to suppress dark current and maintain high photocurrent. *ACS Appl. Mater. Interfaces* **2020,** *12* (23), 26153-26160.

5. Saleem, M. I.; Kyaw, A. K. K.; Hur, J., Infrared Photodetectors: Recent Advances and Challenges Toward Innovation for Image Sensing Applications. *Advanced Optical Materials* **2024,** *12* (33), 2401625.

6. Sulaman, M.; Yang, S.; Guo, H.; Li, C.; Imran, A.; Bukhtiar, A.; Qasim, M.; Ge, Z.; Song, Y.; Jiang, Y.; Zou, B., Synergetic enhancement of CsPbI3 nanorod-based high-performance photodetectors via PbSe quantum dot interface engineering. *Chemical Science* **2024,** *15* (22), 8514-8529.

7. Shafique, S.; Qadir, A.; Iqbal, T.; Sulaman, M.; Yang, L.; Hou, Y.; Miao, Y.; Wu, J.; Wang, Y.; Zheng, F.; Wang, X.; Hu, Z., High-performance self-powered perovskite photodetectors enabled by Nb2CTx-passivated buried interface. *J. Alloys Compd.* **2024,** *1004*, 175903.

8. Saleem, M. I.; Batool, A.; Hur, J., Cutting-Edge Developments in Metal Halide Perovskites Core/Shell Heterocrystals: from Photodetectors to Biomedical Applications. *Small* **2025,** *21* (2), 2407032.

9. Li, Z.; Yan, T.; Fang, X., Low-dimensional wide-bandgap semiconductors for UV photodetectors. *Nat. Rev. Mater.* **2023,** *8* (9), 587-603.

View Article Online
DOI: 10.1039/D5CE00591D

10. Shan, Q.; Dong, Y.; Xiang, H.; Yan, D.; Hu, T.; Yuan, B.; Zhu, H.; Wang, Y.; Zeng, H., Perovskite Quantum Dots for the Next-Generation Displays: Progress and Prospect. *Adv. Funct. Mater.* **2024,** *34* (36), 2401284.

11. Bai, Y.; Hao, M.; Ding, S.; Chen, P.; Wang, L., Surface Chemistry Engineering of Perovskite Quantum Dots: Strategies, Applications, and Perspectives. *Adv. Mater.* **2022,** *34* (4), 2105958.

12. Rainò, G.; Yazdani, N.; Boehme, S. C.; Kober-Czerny, M.; Zhu, C.; Krieg, F.; Rossell, M. D.; Erni, R.; Wood, V.; Infante, I.; Kovalenko, M. V., Ultra-narrow room-temperature emission from single CsPbBr3 perovskite quantum dots. *Nat. Commun.* **2022,** *13* (1), 2587.

13. Kazes, M.; Nakar, D.; Cherniukh, I.; Bodnarchuk, M. I.; Feld, L. G.; Zhu, C.; Amgar, D.; Rainò, G.; Kovalenko, M. V.; Oron, D., Observation of Three-Photon Cascaded Emission from Triexcitons in Giant CsPbBr3 Quantum Dots at Room Temperature. *Nano Lett.* **2024,** *24* (42), 13185-13191.

14. Yan, W.; Shen, J.; Zhu, Y.; Gong, Y.; Zhu, J.; Wen, Z.; Li, C., CsPbBr 3 quantum dots photodetectors boosting carrier transport via molecular engineering strategy. *Nano Res.* **2021**, 1-8.

15. Kazes, M.; Udayabhaskararao, T.; Dey, S.; Oron, D., Effect of surface ligands in perovskite nanocrystals: Extending in and reaching out. *Acc. Chem. Res.* **2021,** *54* (6), 1409-1418.

16. Song, S.; Lv, Y.; Cao, B.; Wang, W., Surface modification strategy synthesized CsPbX3 perovskite quantum dots with excellent stability and optical properties in water. *Adv. Funct. Mater.* **2023,** *33* (21), 2300493.

17. Panigrahi, A.; Kumar, A.; Mishra, L.; Parida, P.; Sarangi, M. K., Hole-Induced Charge Transfer Dynamics at the CsPbBr3 Perovskite Quantum Dot Interface. *J. Phys. Chem. C* **2024,** *128* (41), 17503-17512.

18. Tiede, D. O.; Romero-Pérez, C.; Koch, K. A.; Ucer, K. B.; Calvo, M. E.; Srimath Kandada, A. R.; Galisteo-López, J. F.; Míguez, H., Effect of connectivity on the carrier transport and recombination dynamics of perovskite quantum-dot networks. *ACS Nano* **2024,** *18* (3), 2325-2334.

19. Alosaimi, G.; Huang, C.-Y.; Sharma, P.; Wu, T.; Seidel, J., Morphology-Dependent Charge Carrier Dynamics and Ion Migration Behavior of CsPbBr3 Halide Perovskite Quantum Dot Films. *Small* **2023,** *19* (20), 2207220.

20. Clinckemalie, L.; Valli, D.; Roeffaers, M. B.; Hofkens, J.; Pradhan, B.; Debroye, E., Challenges and opportunities for CsPbBr3 perovskites in low-and high-energy radiation detection. *ACS Energy Lett.* **2021,** *6* (4), 1290-1314.

21. Deng, J.; Yuan, S.; Xiong, H.; Ma, Z.; Wu, W.; Wang, M.; Lou, Z.; Fan, J.; Li, W., Br-I ordered CsPbBr2I perovskite single crystal toward extremely high mobility. *Chem* **2023,** *9* (7), 1929-1944.

22. Xuan, W.; Zheng, L.; Cao, L.; Miao, S.; Hu, D.; Zhu, L.; Zhao, Y.; Qiang, Y.; Gu, X.; Huang, S., Machine learning-assisted sensor based on CsPbBr3@ ZnO nanocrystals for identifying methanol in mixed environments. *ACS Sens.* **2023,** *8* (3), 1252-1260.

View Article Online
DOI: 10.1039/D5CE00591D

23. Liu, J.; Liu, F.; Liu, H.; Yue, J.; Jin, J.; Impundu, J.; Liu, H.; Yang, Z.; Peng, Z.; Wei, H.; Jiang, C.; Li, Y. J.; Xie, L.; Sun, L., Mixed-dimensional CsPbBr3@ZnO heterostructures for high-performance p-n diodes and photodetectors. *Nano Today* **2021,** *36*, 101055.

24. Wang, S.; Yang, S.; Xu, Z.; Xu, H.; Duan, G.; Zhao, D.; Wang, X.; Cao, B., A high-performance photodetector based on a ZnO/CsPbBr3 quantum-dot-level-contact hybrid sandwich structure. *J. Mater. Chem. C* **2025,** *13* (2), 902-909.

25. Yi, G.-C.; Wang, C.; Park, W. I., ZnO nanorods: synthesis, characterization and applications. *Semiconductor Science and Technology* **2005,** *20* (4), S22.

26. Wang, H.; Zhang, P.; Zang, Z., High performance CsPbBr3 quantum dots photodetectors by using zinc oxide nanorods arrays as an electron-transport layer. *Appl. Phys. Lett.* **2020,** *116* (16).

27. Subramaniam, M. R.; Pramod, A. K.; Hevia, S. A.; Batabyal, S. K., Enhanced photoluminescence quantum yield, lifetime, and photodetector responsivity of CsPbBr3 quantum dots via antimony tribromide post-treatment. *J. Phys. Chem. C* **2022,** *126* (3), 1462-1470.

28. Bapathi, K. S. R.; Abdelbar, M. F.; Jevasuwan, W.; Zhang, Q.; Borse, P. H.; Badhulika, S.; Fukata, N., Enhancing silicon photodetector performance through spectral downshifting using core-shell CdZnS/ZnS and perovskite CsPbBr3 quantum dots. *Nano Energy* **2024,** *128*, 109832.

29. Chen, K.; Zhang, X.; Chen, P. A.; Guo, J.; He, M.; Chen, Y.; Qiu, X.; Liu, Y.; Chen, H.; Zeng, Z., Solution-Processed CsPbBr3 Quantum Dots/Organic

Semiconductor Planar Heterojunctions for High-Performance Photodetectors. *Adv. Sci* **2022,** *9* (12), 2105856.

30. Lee, D. J.; Kumar, G. M.; Kim, Y.; Yang, W.; Kim, D. Y.; Kang, T. W.; Ilanchezhiyan, P., Hybrid CsPbBr3 quantum dots decorated two dimensional MoO3 nanosheets photodetectors with enhanced performance. *Journal of Materials Research and Technology* **2022,** *18*, 4946-4955.

31. Yang, B.; Guo, P.; Hao, D.; Wang, Y.; Li, L.; Dai, S.; Huang, J., Self-powered photodetectors based on CsPbBr3 quantum dots/organic semiconductors/SnO2 heterojunction for weak light detection. *Sci. China Mater.* **2023,** *66* (2), 716-723.

View Article Online
DOI: 10.1039/D5CE00591D

Data availability

The datasets used in this study are available from the corresponding author on reasonable request.